SYNTHESIS AND CHARACTERIZATION OF NEW GRAPHENE NANOCOMPOSITES AND STUDY OF THEIR ANTIBACTERIAL, ANTIFUNGAL AND ANTICANCER ACTIVITY

Reem S. Najm[1], *Mohammed J. Saleh[2], Jamil N. Saleh[2]

[1]*Department of Physiology, Pharmacology and Biochemistry, College of Veterinary Medicine, University of Tikrit, Salahuddin-Tikrit, Iraq*
[2] *Salah al-Din Education Directorate, Ministry of Education, Iraq*
**e-mail: Mohammedjwhersaleh96@gmail.com*

Received 04.05.2025
Accepted 11.07.2025

Abstract: *Oncology extensively uses nanographene, an inorganic nanocomposite material, because of its ability to deliver drugs, its adaptability, and its photothermal and photodynamic effects. However, the restricted use of the abovementioned features limits its current use. This is mainly because graphene oxide nanoparticles' physical and chemical characteristics are poorly understood. Two nanocomposites, R1, were formed by reacting graphite nanocellulose with prepared triazole nanocellulose, and R2, by reacting graphene oxide with graphene triazole nanocellulose. Ultrasound and dioxane were used as solvents in both methods. The nanoscale properties of the composites were verified using scanning electron microscopy (SEM), atomic force microscopy (AFM), and X-ray diffraction (XRD). The bacterial susceptibility of the composites was tested against two types of gram-positive bacteria, Staphylococcus aureus and gram-negative Escherichia coli, using the antibiotic ampicillin as a control sample. The composites had a high inhibitory activity compared to the antibiotic. The effect of the composites on a type of fungus, Candida albicans, was also investigated, using the antibiotic itraconazole as a control sample. The composites demonstrated inhibitory activity. Higher fungal activity than antibiotics, and the anticancer activity was tested against MCF-7 breast cancer cells at five concentrations (31.2, 62.5, 125, 250, and 500 micrograms/ml), showing good inhibitory activity.*
Keywords*: nanocomposites, graphene, antibacterial activity, Fungal Biological, Breast cancer*
DOI: 10.65382/2221-8688-2026-3-333-345

1. Introduction

Cancer has long posed a serious risk to people's health since it is a fatal illness [1]. How cancer is treated has changed significantly in the last several decades. Today, a complete treatment strategy that combines biological targeted therapy, chemotherapy, radiation, and surgery is used to treat cancer. Nevertheless, each of the therapies above has drawbacks. Patients with tumors still have an abysmal five-year survival rate. Clinical experience has demonstrated that most current medicines cannot increase the cure rate of cancer patients, except a few specialized medications [2]. Individuals are searching for more cancer treatment programs to enhance the current cancer treatment system. Nanomaterials have gained popularity in anticancer research in recent years. Graphene nanocomposites stand out among nanomaterials because of their distinct physicochemical characteristics [3]. Graphane (hydrogenated graphene), fluorographene (fluorinated graphene), graphdiyne, porous graphene, graphene nanoribbon (GNR), graphene oxide (GO), and reduced graphene oxide (rGO) are some of the several kinds of graphene-based materials that have been created thus far [4]. GO and rGO are most often utilized in biological applications, including theranostics in oncology, imaging agent distribution, and anticancer medication carriers [5]. The modified Hummer's technique is frequently used to create graphene oxide (GO), a highly oxidized version of graphene. The proper reducing agents are added to GO to create rGO [6]. Currently, graphene materials are often employed in clinical and biological settings as graphene nanocomposites. Additionally, graphene materials possess antifungal [7] and antibacterial properties [8]. The goal of our study is to create

graphene nanocomposites and investigate their potential as a treatment for cancer cells, fungus, and bacteria.

2. Experimental part

2.1. Devices used. The Electrothermal Melting Apparatus 9300 measured the melting points. FT-IR 8400S Shimadzu spectrophotometer by KBr disc, 400–4000 cm-1 scale. The Raypa steam sterilizer (Spain) autoclave at the University of Tikrit's Advanced Microbiology Research Laboratory was utilized to sterilize the microbiological medium used in the study. Petri dishes utilized for the microbiological investigation were incubated in the same lab using a Heraeus D-63450 incubator (Germany). Atomic Force Microscopy (AFM) was carried out at Kashan University in Iran using a US AFM Icon equipment. Scanning Electron Microscopy (SEM) was carried out using a MIRA3-TE SCAN microscope from Belsorp, Czech Republic. A Shimadze-XRD-6000 instrument was used for X-Ray Diffraction (XRD) analysis at Kashan University in Iran.

2.2. Synthesis of Nano-graphene composite (R1) [9, 10]. Following the dissolution of 1 g of the produced nanographite cellulose in 15 ml of dioxane, the solution was homogenized (free of plankton) using ultrasound. It was then filtered, washed with distilled water, and dried at 70°C after 1 g of the produced nanocellulosegraphene triazole was placed in an ice bath at 0°C and increased for 30 minutes with magnetic stirring.

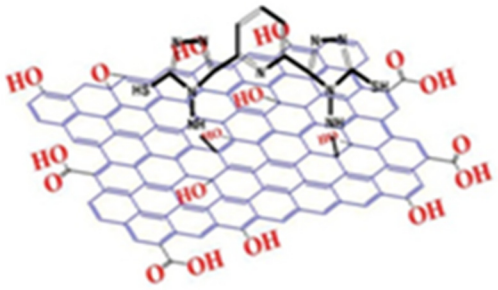

2.3. Synthesis of Nano-reduced graphene oxide (R2) [9, 10]. Fifteen milliliters of dioxane were used to dissolve (1 g) the manufactured nano-reduced graphene oxide. Ultrasound was used to homogenize the solution until it was homogenous, or a clear solution devoid of plankton. Subsequently, 1 gram of the synthesized nano-cellulose graphene triazole was put into an ice bath at 0°C, magnetically agitated for 30 minutes, filtered, cleaned with distilled water, and allowed to dry at 70°C.

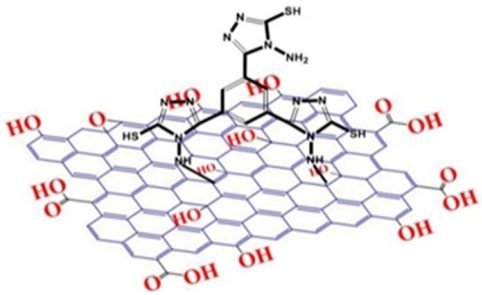

2.4. Evaluation of bacterial bioactivity. Two bacterial strains, Gram-positive *Staphylococcus aureus* and Gram-negative *Escherichia coli*, were obtained from the central laboratories of Tikrit University. The Mueller–Hinton agar culture medium was prepared by dissolving 20 g of the medium in 500 mL of water, followed by stirring and sterilization in an autoclave at 1.5 bar and 120°C for 14 minutes.

After cooling, the medium was poured into Petri dishes and allowed to solidify at 25°C [11].

Solutions of the nanocomposites R1 and R2 were prepared in DMSO at three concentrations (0.01, 0.001, and 0.0001 mg/mL). The agar plates were inoculated by streaking the bacterial cultures in three directions to ensure uniform distribution. Wells (6 mm in diameter) were then punched into the agar using a sterile cork borer, and the test solutions were added to the wells. The plates were incubated at 37°C for 24 hours in a controlled environment. The zones of inhibition were measured in millimeters using a ruler, with ampicillin serving as the control antibiotic [12, 13].

2.5. Evaluation of Fungal Biological Activity. In the laboratories of Tikrit University, one *Candida albicans* species was prepared. Fifteen grams of medium spears were dissolved in half a liter of water and placed in an autoclave under 1.5 bar pressure for 14 minutes at 122°C. The solution was then cooled, poured into plates, and left to dry at 25°C. The solution concentrations were prepared differently from the bacterial activity, with four concentrations (25, 50, 75, and 100 mg/ml) in DMSO. The fungi were then swept from the center in three directions to obtain the largest surface area, and three holes were found in each plate using a 6 mm diameter cork piercer. The solutions were poured into each hole, incubated in an incubator, and mixed for two weeks. The results were read using a mm diameter ruler. The antibiotic *itraconazole* was used as a control [14, 15].

2.4. Cytotoxicity test for breast cancer (MCF-7). Breast cancer cells were prepared from Kashan University, Iran. Cell suspensions at a concentration of 1×10^4 to 1×10^6 cells/ml were prepared in a 96-well plate with a final volume of 200 µl of complete medium per well. The plates were covered with sterile parafilm, gently agitated, and incubated in a 5% CO_2 incubator at 37°C for 24 h. Following incubation, the medium was discarded, and three wells were filled with 200 µl of the produced concentrations of the investigational drugs [R1, R2] (31.2, 62.5, 125, 250, and 500 µg/ml). After adding control samples, the mixture was incubated for 24 hours at 370°C in an incubator with 5% CO_2. Following the incubation of the plates with the compounds under investigation [R1, R2], 10 µL of MTT solution was added to each well, and the plates were then incubated for 4 hours at 37°C in an incubator with 5% CO_2. Each well received 100 µL of DMSO dissolving solution, which was then incubated for five minutes. An ELISA device was used to measure the absorbance at 570 nm [16, 17].

3. Results and discussions

3.1. Characterization of R1 nanocomposite. The FT-IR spectrum of the R1 nanocomposite showed two bands at (3294, 3279) cm^{-1} attributed to the (NH_2) bond and their overlap with the (OH) band appearing at the same position (3294) cm^{-1}.

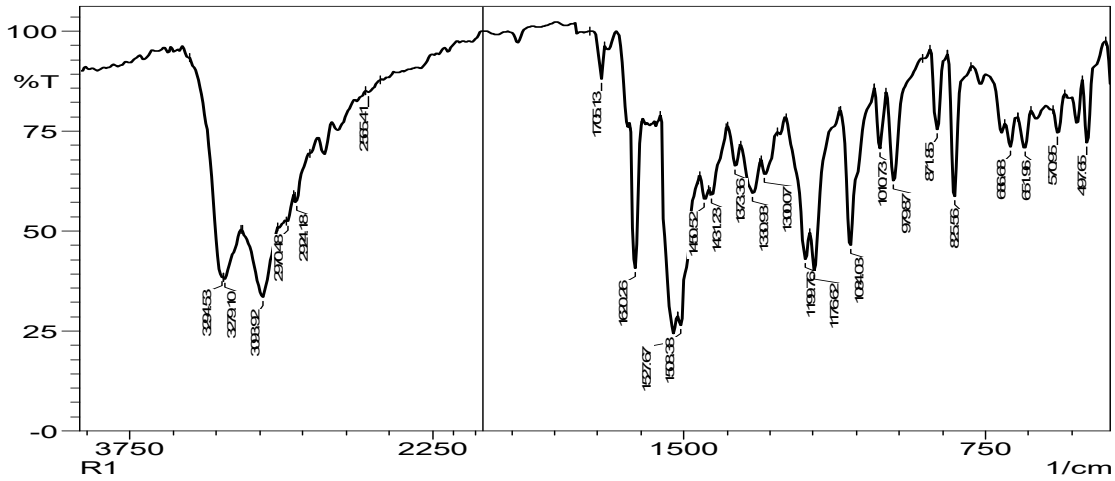

Fig. 1. FT-IR spectrum of the R1 nanocomposite

The spectrum showed a band at (3093) cm^{-1} typically associated with the (Ar-CH) bond, in addition to two other bands at (2970, 2904) cm^{-1} attributed to the aliphatic (CH) group, and a band at (2565) cm^{-1} attributed to the (SH) group. The spectrum also showed a band at (1705) cm^{-1} typically associated with the (C=O) group, a band at (1620) cm^{-1} typically associated with the azimethine (C=N) group in the triazole ring, and a band at (1300) cm^{-1} typically associated with the (C-N) group [18] (Fig. 1). Fig. 2 shows the X-ray diffraction spectrum of compound R1. The main diffraction peak appears at $2\theta = 29.385°$, corresponding to an interlayer spacing (d) of 0.3037 nm, a grain size (D) of 2.8 nm, and an estimated number of layers (n) of 9.3. These values are consistent with previously reported data [19].

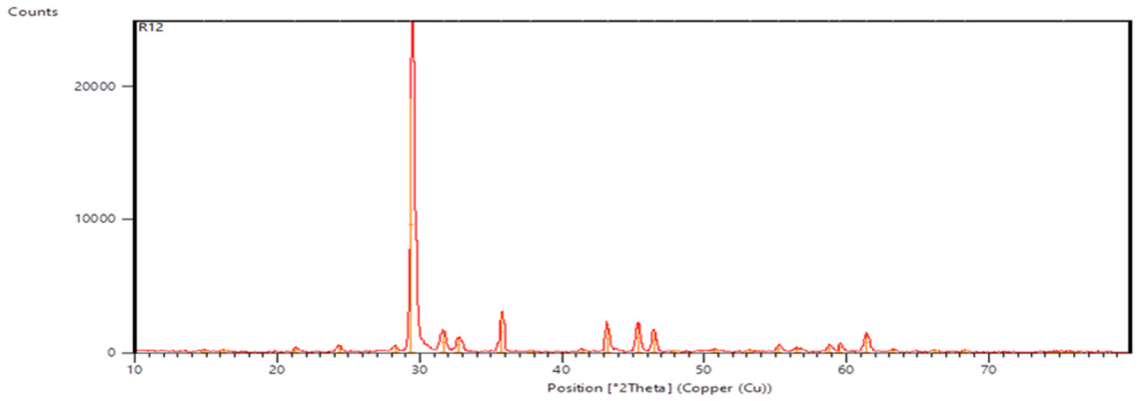

Fig. 2. XRD pattern of the R1 nanocomposite

Fig. 3 presents the morphological analysis of compound R1 obtained by field emission scanning electron microscopy (FESEM). The images reveal several notable features:

- *Particle distribution:* The observed dispersion suggests the formation of nanoparticles as a result of the reaction.
- *Homogeneous distribution:* The uniformity of the particles indicates good interaction among the nanocomposites, which can enhance their practical performance.
- *Particle size:* The small particle dimensions are consistent with nanoscale behavior, potentially improving antimicrobial activity.
- *Shape and structure:* Variations in particle morphology may reflect specific chemical interactions between the components, which can influence the physical and chemical properties of the final material.
- *Dispersion on the surface:* The even spread of particles across the surface may affect the efficiency of applications such as catalysis or biological processes [20].

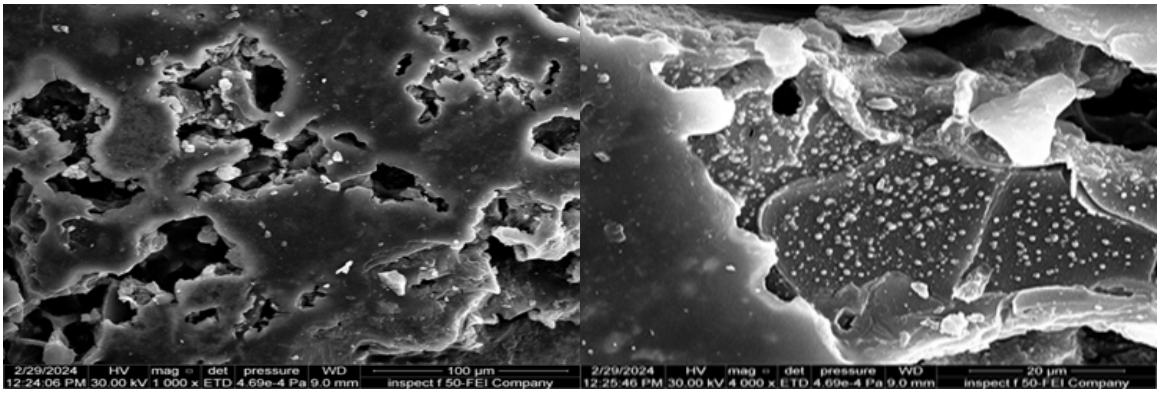

a **b**

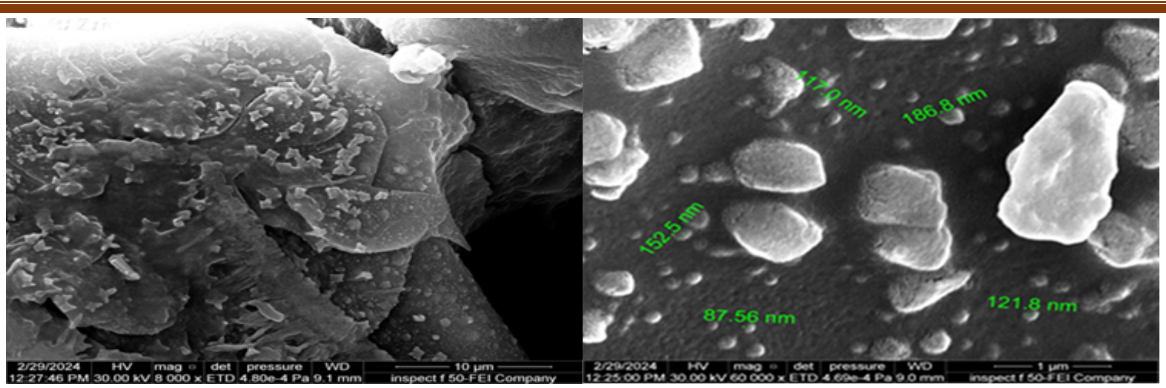

c d

Fig. 3. FESEM images of the R1 nanocomposite

Fig. 4 shows the morphological analysis of compound R1 obtained by atomic force microscopy (AFM). The images reveal the size and distribution of nanoparticles across the surface of the extract, with several notable features:

- *Homogeneous surface distribution:* The particles are evenly dispersed across the surface (image a), including along the rims.
- *Cavities and surface defects:* Distinct cavities and irregularities are visible (image b), which may affect surface reactivity.
- *Formation of peaks:* The AFM images display nanoscale peaks (image c) resembling volcanic structures, indicating localized growth or aggregation.
- *Layer connectivity and sheet morphology:* The parallel arrangement of nanosheets (image d) exhibits clear zigzag peeling, while the rims of stratified clusters show connected layers, suggesting structural rearrangement at the nanoscale [21].

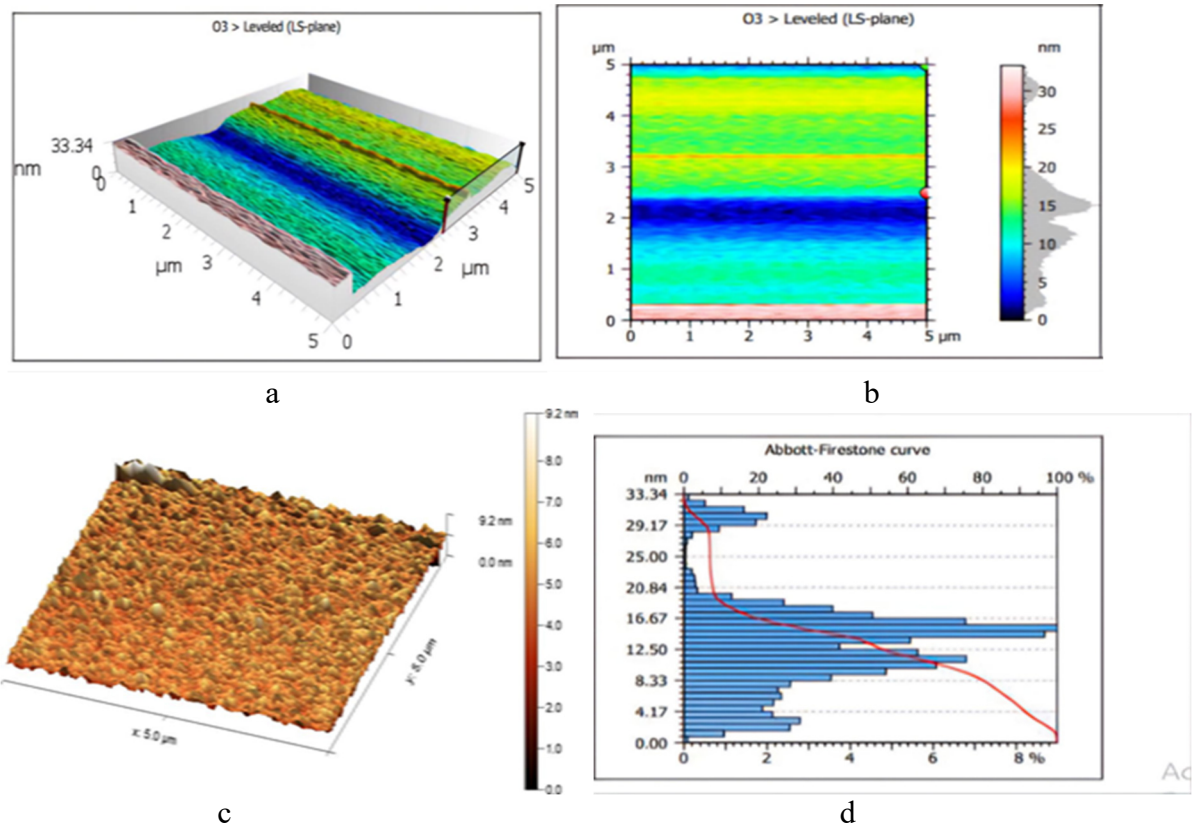

a b

c d

Fig. 4. AFM images for the R1 nanocomposite

3.2. Characterization of R1 nanocomposite. The FT-IR spectrum of the R2 nanocomposite showed that the presence of two bands at (3271, 3313) cm^{-1} is attributed to the

(NH_2) bond and its overlap with the (OH) band that appears at the same position (3313) cm^{-1}. The spectrum also showed a band at position (3213) cm^{-1} attributed to the (NH) group. The spectrum showed a band at position (3051) cm^{-1} usually associated with the (Ar-CH) bond, in addition to two other bands at positions (2816, 2920) cm^{-1} attributed to the aliphatic (CH) group, and a band at position (2596) cm^{-1} attributed to the (SH) group. The spectrum also showed a band at position (1701) cm^{-1} that was usually associated with the (C=O) group, a band at position (1631) cm^{-1} that was traditionally associated with the azamethine (C=N) group in the triazole ring, and a band at position (1276) cm^{-1} that was usually associated with the (C-N) group [22] (Fig. 5).

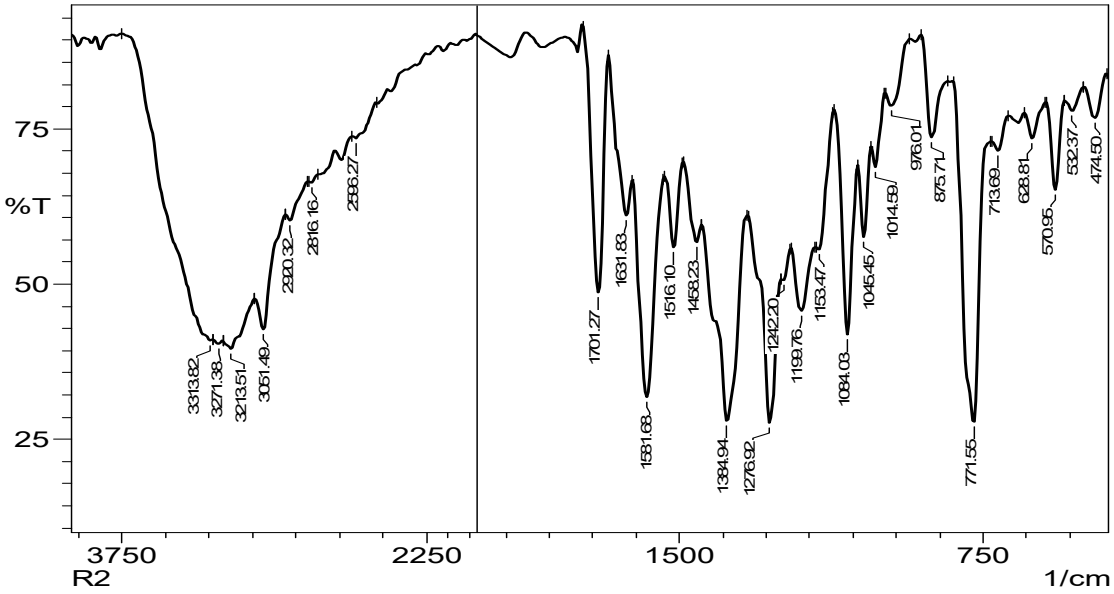

Fig. 5. FT-IR spectrum of the R2 nanocomposite

Fig. 6 shows the X-ray diffraction spectrum of compound R2. The diffraction peak appears at 2θ = 22.8°, corresponding to an interlayer spacing (d) of 0.202 nm. The calculated grain size (D) is approximately 1.5 nm, and the estimated number of layers (n) is about 2.1. These values are consistent with those previously reported in the literature [19].

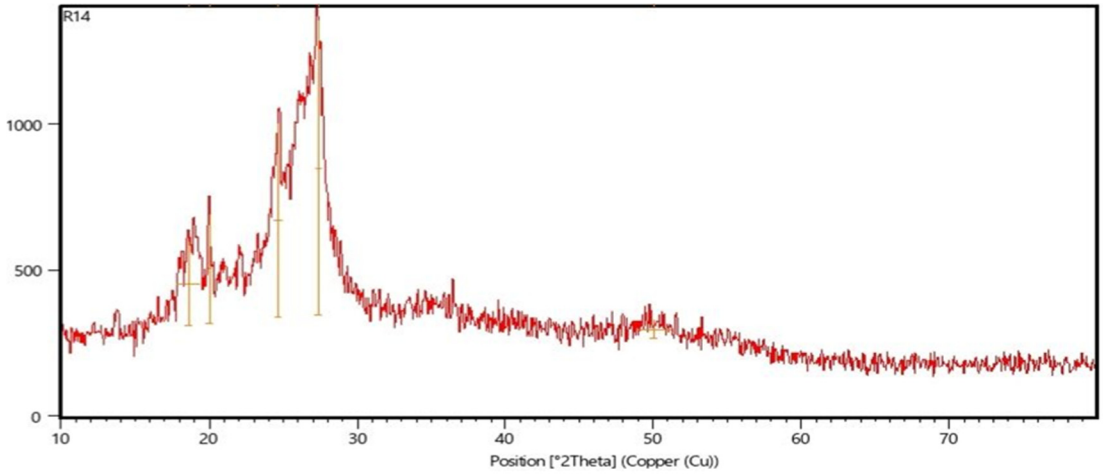

Fig. 6. XRD spectrum for the R2 nanocomposite

Fig. 7 shows the field emission scanning electron microscopy (FESEM) images of compound R2. The micrographs reveal increased porosity, larger particle size, and an expanded surface area, along with a pronounced and well-defined stratification of triazole layers. In image

(a), sheet thickening is evident, while images (b) and (c) show surface cracks on the peeled sheets and the formation of deep cavities. Image (d) highlights the rough surface morphology, which can be attributed to the intrinsic structural characteristics of the compound [23].

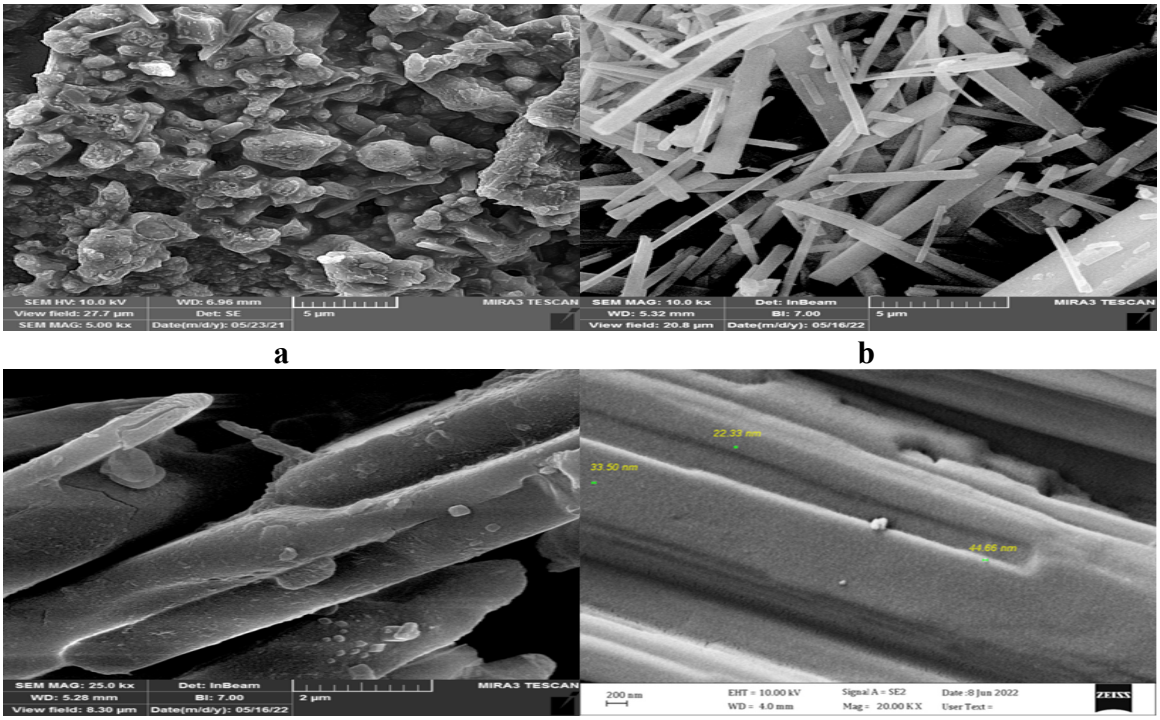

Fig. 7. FESEM images for the R2 nanocomposite

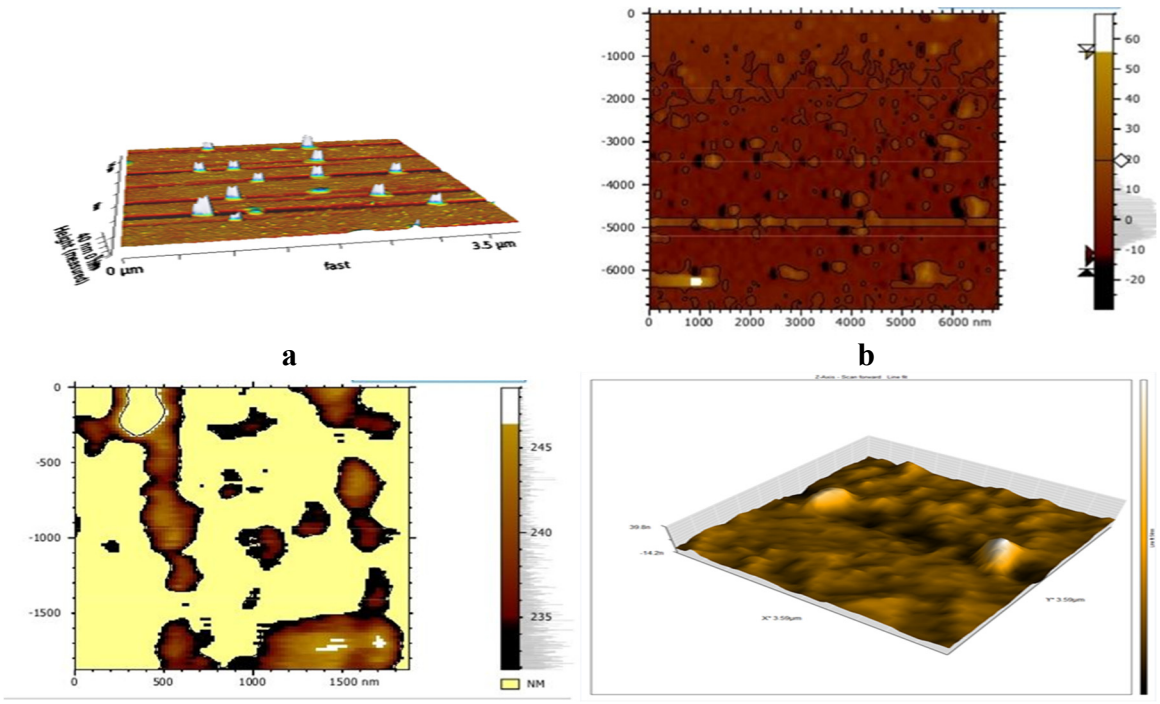

Fig. 8. AFM images for the R2 nanocomposite

Fig. 8 presents the atomic force microscopy (AFM) images of compound R2. The micrographs reveal a series of parallel, interconnected peaks, suggesting the role of amine groups in enhancing exfoliation and promoting the formation of additional graphene-

like sheets. The edges of these sheets exhibit pronounced elevations attributed to triazole moieties. Image (a) displays a uniform distribution across the surface and edges, while images (b) and (c) reveal the presence of cavities and structural defects. Image (d) shows a recurring pattern in the morphology of the formed peaks, further supporting the observed exfoliation effect.

3.3. Evaluation of bacterial bioactivity. By measuring the diameter of inhibition in mm, it was found that compound R1 showed the highest inhibition at a concentration of 0.01 against *Staphylococcus aureus* bacteria with a diameter of 25 mm, which is higher than the used antibiotic. At a concentration of 0.001, it showed a 20 mm diameter of inhibition, while at 0.0001, it showed 15 mm. As for *Escherichia coli* bacteria only, this compound showed a diameter of inhibition of 20 mm at a concentration of 0.01, equal to the used drug. This inhibition decreased to 15 mm at a concentration of 0.001, and the lowest inhibition appeared at a concentration of 0.0001 with a diameter of 10 mm. It is clear that compound R1 showed a high effectiveness against positive bacteria compared to negative bacteria. This is due to the nature of the cell membrane, as negative bacteria have a more complex membrane than positive bacteria [24, 25]. As for compound R2, it showed inhibitory activity against positive bacteria. *Staphylococcus aureus* inhibition diameter of 23 mm at 0.01 concentration is superior to the antibiotic but less than the compound R1. Equivalent inhibition with R1 reaches 20 mm at 0.001 concentration.

Table 1. Antibacterial activity of the synthesized compounds (inhibition zone in mm)

Com. No	***Staph. aureus* mg/ml**			***E. coli* mg/ml**		
	0.01	**0.001**	**0.0001**	**0.01**	**0.001**	**0.0001**
R 1	25	20	15	20	15	10
R 2	23	20	14	21	16	13
Ampicillin.	22	18	15	20	17	14

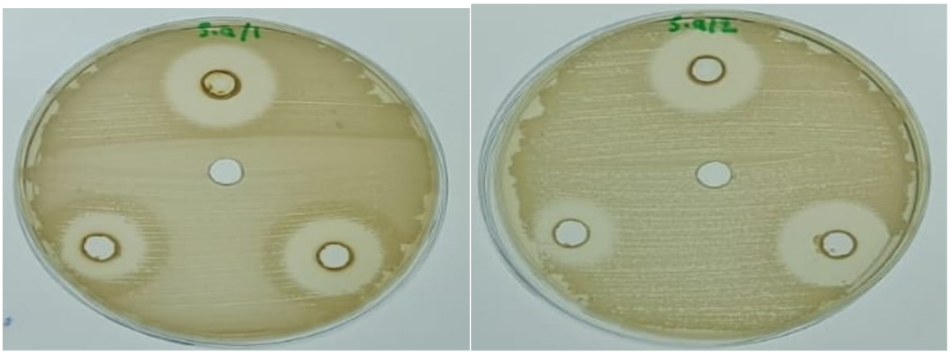

Fig. 9. Efficacy of the nanocomposite (R1, R2) against *Staphylococcus aureus* bacteria

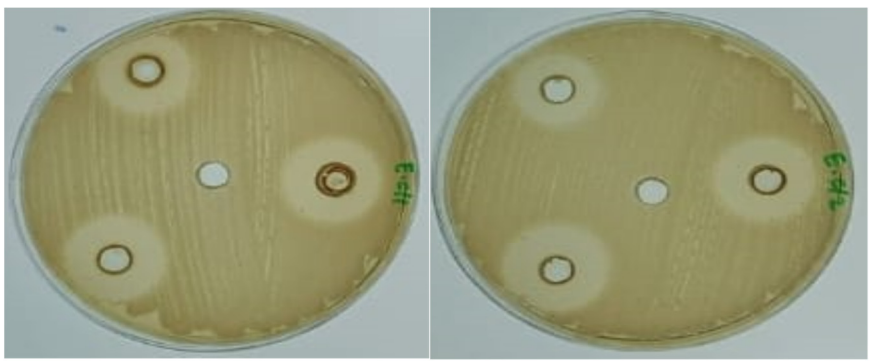

Fig. 10. Efficacy of the nanocomposite (R1, R2) against *Escherichia coli* bacteria

This inhibition also decreases at 0.001 concentration to 14 mm. It gave the highest inhibition against gram-negative bacteria *Escherichia coli* at high concentrations of 21

mm, which is superior to the antibiotic and compound R1. At intermediate concentrations, it showed 16 mm inhibition, and at low concentrations, 13 mm showed an inhibition diameter higher than that of compound R1 in both cases [26]. The results of this compound R2 demonstrate its ability to penetrate the membrane of the gram-negative cell, which gives hope that it may be a future antibiotic. It is noted that inhibition increases with increasing inhibition diameter, as the compounds showed the highest inhibition after high concentrations [27, 28] (Table 1, Fig. 9 and 10).

3.4. Evaluation of antifungal bioactivity. When studying the inhibitory effectiveness of nanocomposites against the fungus *Candida albicans*, we note the presence of a direct relationship between the concentration and the diameter of inhibition in both compounds, as the prepared compounds gave the highest effectiveness at a concentration of 100 mg/ml with an effectiveness of 16 mm for R1 and 20 for R2, where the effectiveness of compound R2 is close to the drug used, making it more effective than compound R1. In comparison, at a concentration of 75 mg/ml, compound R1 showed effectiveness with an inhibition diameter of 14 mm, and compound R2 with a diameter of 16 mm, making it closer to the effectiveness of the drug, which showed effectiveness with a diameter of 18 mm [29, 30]. As for the concentration of 50 mg/ml, compound R1 showed effectiveness with a diameter of 12 mm, which is less than that of compound R2, which reaches 15 mm, equal to the drug's effectiveness. At low concentrations of 25 mg/ml, compound R1 was effective with a diameter of 11 mm. In contrast, compound R2 gave effectiveness equal to the drug, with an inhibition diameter that reached 13 mm. However, the drug was slightly more effective than the nanocomposites; it was still very effective, with the R2 complex being close to the drug's effectiveness, which gives hope for the possibility of using it as an antibiotic against fungi [31, 32] (Table 2, Fig. 11).

Table 2. Fungal bioactivity results of the prepared compounds and antibiotics (mm)

Comp No.	*Candida albicans mg/ml*			
	100	**75**	**50**	**25**
R 1	16	14	12	11
R 2	20	16	15	13
Itraconazole	22	18	15	13

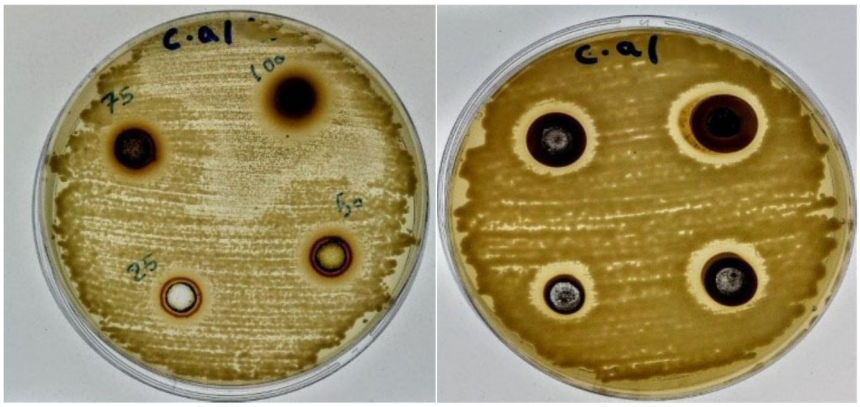

Fig. 11. Efficacy of nanocomposites (R1, R2) against *Candida albicans*

3.5. Cytotoxicity test for breast cancer (MCF-7). When studying the effect of nanocomposites R1 and R2 on cancer cells, it was found that there is an inverse relationship between the concentration and the survival rate of cancer cells. For nanocomposite R1, at low concentrations such as 31.2 µg/ml, the survival rate was 87% of the cells and began to decrease as the concentration increased, reaching 80% at 62.5 µg/ml. At a concentration of 125 µg/ml, it was 84%, and at a concentration of 200 µg/ml, it reached 78%. The best results appeared at a concentration of 500, as the cell survival rate reached 43%, meaning that more than half of the cells were affected by this nanocomposite. This indicates its medical importance at high

concentrations or its combination with other treatments to increase the effect on cancer cells. As shown in Figures 12 and 13, compound R2 showed similar results to compound R1, but with a slightly better survival rate. It showed a cell survival rate of 85% at 31.2 µg/ml, a 78% survival rate at 62.5 µg/ml, a 67% survival rate at 125 µg/ml, and a 57% survival rate at 200 µg/ml. The best results were found at the highest concentration, with a 41% survival rate at 500 µg/ml, demonstrating its potential as an anticancer drug, as shown in Figures 14 and 15. These results indicate that both compounds have moderate anticancer activity, but compound R1 exhibits slightly higher activity. These data may encourage further research to improve the properties of both compounds and enhance their efficacy by modifying their chemical structures or testing them in other therapeutic formulations [33, 34].

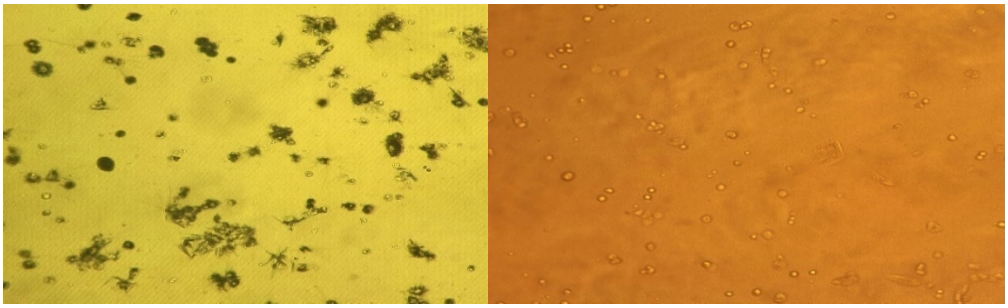

Fig. 12. Effect of nanocomposite R1 on MCF-7 cells

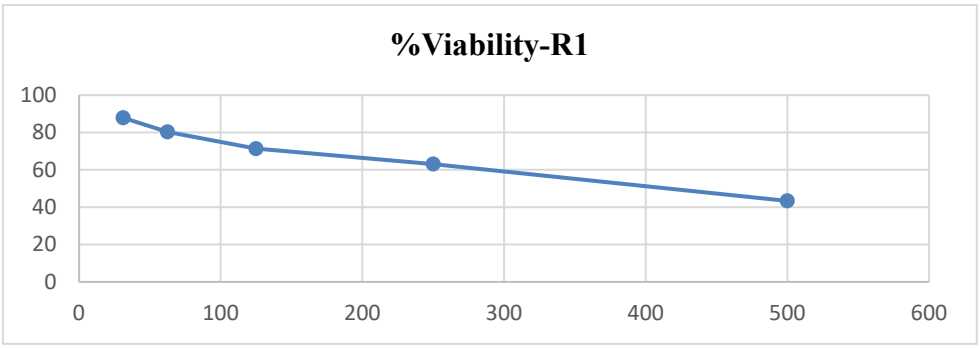

Fig. 13. Effect of nanocomposite R1 on MCF-7 cells and HdFn cells using MTT assay

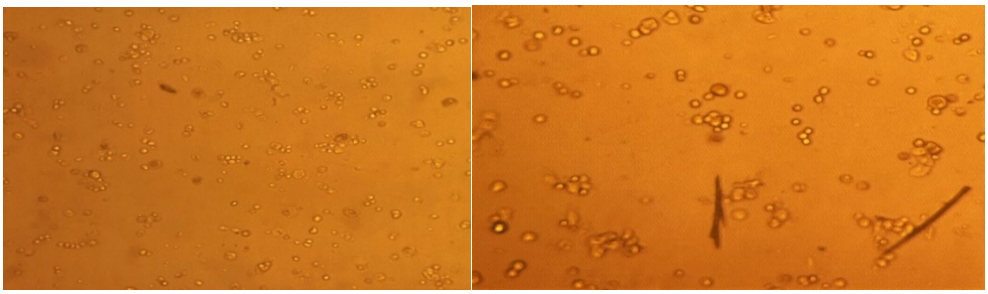

Fig. 14. Effect of nanocomposite R1 on MCF-7 cells

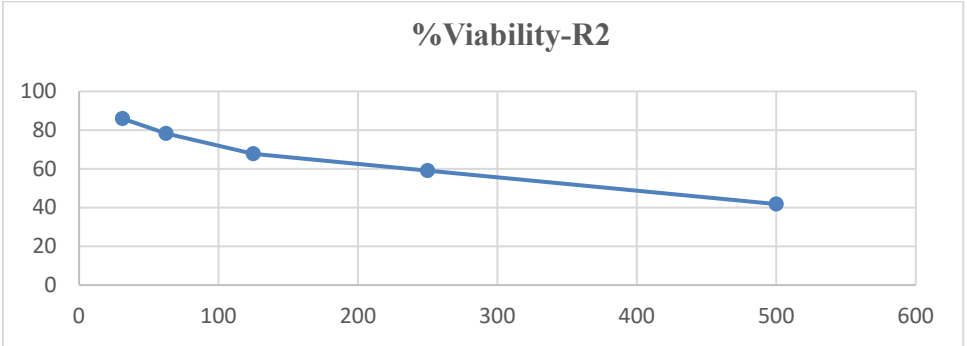

Fig. 15. Effect of nanocomposite R2 on MCF-7 cells and HdFn cells using MTT assay

4. Conclusions

Two nanocomposites, R1 and R2, were synthesized, and their nanostructure, particle size, and surface area were confirmed using SEM, AFM, and XRD analyses, demonstrating that the composites possess nanoscale features. Infrared spectroscopy further verified their structural integrity. Both nanocomposites exhibited pronounced antibacterial activity: compound R1 demonstrated superior efficacy compared to standard antibiotics against *Staphylococcus aureus*, indicating its potential as an alternative therapeutic agent. Compound R2 showed higher activity than ampicillin against *Escherichia coli*, confirming its potential use as an antibacterial agent against this pathogen. Evaluation of antifungal activity against *Candida albicans* revealed that both nanocomposites displayed comparable efficacy, with R2 performing slightly better, approaching the effectiveness of *itraconazole* at both low and high concentrations, and achieving equivalent performance at higher concentrations. Furthermore, cytotoxicity studies against cancer cells indicated that both nanocomposites significantly reduced cell survival rates by more than 50%, highlighting their promise as candidates for the development of anticancer therapies.

References

1. Duggan S.T., Keating G.M. Pegylated liposomal doxorubicin: a review of its use in metastatic breast cancer, ovarian cancer, multiple myeloma and AIDS-related Kaposi's sarcoma. *Drugs*, 2011, **Vol. 71**, p. 2531-2558. DOI: 10.2165/11207510-000000000-00000
2. Allemani C., Matsuda T., Di Carlo V., Harewood R., Matz M., Nikšić M., Bonaventure A., Valkov M., Johnson C.J., Estève J., Ogunbiyi O.J., E Silva G.A., Chen W.-Q., Eser S., Engholm G., Stiller Ch.A., Monnereau A., Woods R.R., Visser O., Lim G.H., Aitken J., Weir H.K., Hood M. Global surveillance of trends in cancer survival 2000–14 (CONCORD-3): analysis of individual records for 37 513 025 patients diagnosed with one of 18 cancers from 322 population-based registries in 71 countries. *The Lancet*, 2018, **Vol. 10125**, p. 1023-1075. DOI: 10.1016/s0140-6736(17)33326-3
3. Qu Y., He F., Yu C., Liang X., Liang D., Ma L., Zhang Q., Lv J., Wu J. Advances on graphene-based nanomaterials for biomedical applications. *Materials Science and Engineering: C*, 2018, **Vol. 90**, p. 764-780. DOI: 10.1016/j.msec.2018.05.018
4. Yang K., Zhang S., Zhang G., Sun X., Lee S.T., Liu Z. Graphene in mice: ultrahigh in vivo tumor uptake and efficient photothermal therapy. *Nano letters*, 2010, **Vol. 9**, p. 3318-3323. DOI: 10.1021/nl100996u
5. Thapa R.K., Choi J.Y., Poudel B.K., Choi H.G., Yong C.S., Kim J.O. Receptor-targeted, drug-loaded, functionalized graphene oxides for chemotherapy and photothermal therapy. *International journal of nanomedicine*, 2016, **Vol. 7**, p. 2799-2813. DOI: 10.2147/IJN.S105401
6. Liu Z., Zhang J., Tian Y., Zhang L., Han X., Wang Q., Cheng W. Targeted delivery of reduced graphene oxide nanosheets using multifunctional ultrasound nanobubbles for visualization and enhanced photothermal therapy. *International Journal of Nanomedicine*, 2018, **Vol. 12**, p. 7859-7872. DOI: 10.2147/IJN.S181268
7. Gungordu Er.S., Edirisinghe M., Tabish T.A. Graphene-based nanocomposites as antibacterial, antiviral and antifungal agents. *Advanced Healthcare Materials*, 2023, **Vol. 6**, 2201523. DOI: 10.1002/adhm.202201523
8. Ghazzy A., Naik R.R., Shakya A.K. Metal–polymer nanocomposites: A promising approach to antibacterial materials. *Polymers*, 2023, **Vol. 9**, 2167. DOI: 10.3390/polym15092167
9. Salih B.D., Mohammed A.S., Najm R.S., Mahmood A.R., Alheety M.A. Ortho-and Para-Nitrile Substituted Effect of (1H-Indol-2-Yl) Benzonitrile-Boehmite on the Nano Structures, Surface Area and Hydrogen Storage. *Energy Storage*, 2024, **Vol. 6**, e70034. DOI: 10.1002/est2.70034

10. Fu X., Zhu Y., Li J., Jiang L., Zhao X., Fan X. Preparation, characterization and application of nano-graphene-based energetic materials. *Nanomaterials*, 2021, **Vol. 9**, 2374. DOI: 10.3390/nano11092374
11. Murad Z.A., Hamad A.S. Preparation and diagnosis of new derivatives of the tetrazole ring derived from 2-bromoisophthaladehyde and evaluation of their biological effectiveness. *Chemical Problems*, 2025, **Vol. 23(1)**, p. 116-124. DOI: 10.32737/2221-8688-2025-1-116-124
12. Muhammad F.M., Khairallah B.A., Albadrany K.A. Synthesis, characterization and antibacterial evaluation of novel 1, 3-oxazepine derivatives using a cycloaddition approach. *Journal of Angiotherapy*, 2024, **Vol. 3**, p. 1-5. DOI: 10.25163/angiotherapy.839506
13. Abdullah S.H., Salih M.M., Al-Badrany A. Synthesis, Characterization and Antibacterial Evaluation of Novel Thiazolidine Derivatives. *Journal of Angiotherapy*, 2024, **Vol. 3**, p. 1-9. DOI: 10.25163/angiotherapy.839501
14. Saleh M.J., Ahmed S.E., Saleh J.N. Synthesis, Characterization of Tetrazole Derivatives, and Evaluation of Bacterial and Fungal Activity. *Asian Journal of Chemical Sciences*, 2025, **Vol. 2**, p. 123-134. DOI: 10.9734/ajocs/2025/v15i2364
15. Zheng R., Li S., Zhang X., Zhao C. Biological activities of some new secondary metabolites isolated from endophytic fungi: A review study. *International Journal of Molecular Sciences*, 2021, **Vol. 2**, 959. DOI: 10.3390/ijms22020959
16. Mazlumoğlu B.Ş. In vitro cytotoxicity test methods: MTT and NRU. *PharmATA*, 2023, **Vol. 2,** p. 50-53. DOI: 10.5152/pharmata.2023.1287964
17. Verma S., Prabhakar Y.S. Target based drug design-a reality in virtual sphere. *Current medicinal chemistry*, 2015, **Vol. 22(13)**, p. 1603-1630. DOI: 10.2174/0929867322666150209151209
18. Lee M.S., Whang D.R., Choi H.J., Yang M.H., Kim B.G., Baek J.B., Chang D.W. A facile approach to tailoring electrocatalytic activities of imine-rich nitrogen-doped graphene for oxygen reduction reaction. *Carbon*, 2017, **Vol. 122**, p. 515-523. DOI: 10.1016/j.carbon.2017.07.001
19. Najm R.S., Shannak Q.A., Dalaf A.H. Synthesis and Decoration of Aromatic Derivatives Nano Platelets by the Electric Method. *Azerbaijan Pharmaceutical and Pharmacotherapy Journal*, 2023, **Vol. 2**, p. 92-97. DOI: 10.61336/appj/22-2-22
20. Najm R.S., Al-Somaidaie G.H. Carbonation and preparation of reduced graphene oxide sheets from cellulose. In *39th PATTAYA International Conference on "Advances in Chemical, Agriculture, Biology & Environment"(PCABE-22) Pattaya (Thailand).* 2022, **Vol. 25.** DOI: 10.17758/DIRPUB12.DIR0822212
21. Saravanan G., Mohan S. Pt nanoparticles embedded on reduced graphite oxide with excellent electrocatalytic properties. *Applied Surface Science*, 2016, **Vol. 386**, p. 96-102. DOI: 10.1016/j.apsusc.2016.05.152
22. Majeed H.M., Najem R.S., Baqer O.A.M. Evaluations of Antimicrobial Activity of Aqueous, Ethanolic Extracts of Peganumharmala L. Against Pathogenic Bacteria Isolated From. *Systematic Reviews in Pharmacy*, 2020, **Vol. 11(6)**, p. 409-415. DOI: 10.5530/srp.2019.2.04
23. Salih B.D., Mohammed A.S., Najm R.S., Mahmood A.R., Alheety M.A. Ortho-and Para-Nitrile Substituted Effect of (1H-Indol-2-Yl) Benzonitrile-Boehmite on the Nano Structures, Surface Area and Hydrogen Storage. *Energy Storage*, 2024, **Vol. 6**, e70034. DOI: 10.1002/est2.70034
24. Saleh R.H., Rashid W.M., Dalaf A.H., Al-Badrany K.A., Mohammed O.A. Synthesis of some new thiazolidinone compounds derived from schiff bases compounds and evaluation of their laser and biological efficacy. *Ann Trop & Public Health*, 2020, **Vol. 7**, p. 1012-1031. DOI: 10.36295/ASRO.2020.23728
25. Muhammad F.M., Khairallah B.A., Albadrany K.A. Synthesis, characterization and antibacterial evaluation of novel 1, 3-oxazepine derivatives using a cycloaddition approach. *Journal of Angiotherapy*, 2024, **Vol. 3**, p. 1-5. DOI: 10.25163/angiotherapy.839506

26. Khalil S.L., Saleem N.H. Synthesis and characterization of five-membered heterocyclic compounds of tetrazole derivatives and their biological activity. *Chemical Problems*, 2025, **Vol. 23(3)**, p. 365-374. DOI: 10.32737/2221-8688-2025-3-365-374
27. Zhang L., Li D., Chen X., Zhao F. Marine-Derived Diterpenes from 2019 to 2024: Structures, Biological Activities, Synthesis and Potential Applications. *Marine Drugs*, 2025, **Vol. 2**, 72. DOI: 10.3390/md23020072
28. Hassan B.A., Mekky A.H. Synthesis, characterization and antibacterial activity of [1, 2, 4] triazolo [4, 3-b][1, 2, 4, 5] tetrazine derivatives. *Chemical Problems*, 2025, **Vol. 23(1)**, p. 78-94. DOI: 10.32737/2221-8688-2025-1-78-94
29. Chen S., Wang X., Cheng Y., Gao H., Chen X. A review of classification, biosynthesis, biological activities and potential applications of flavonoids. *Molecules*, 2023, **Vol. 13**, 4982. DOI: 10.3390/molecules28134982
30. Ferreira S.B., Sodero A.C., Cardoso M.F., Lima E.S., Kaiser C.R., Silva Jr F.P., Ferreira V.F. Synthesis, biological activity, and molecular modeling studies of 1 h-1, 2, 3-triazole derivatives of carbohydrates as α-glucosidases inhibitors. *Journal of medicinal chemistry*, 2010, **Vol. 6**, p. 2364-2375. DOI: 10.1021/jm901265h
31. Luczynski M., Kudelko A. Synthesis and biological activity of 1, 3, 4-oxadiazoles used in medicine and agriculture. *Applied Sciences*, 2022, **Vol. 8**, 3756. DOI: 10.3390/app12083756
32. Elkanzi N.A., Hrichi H., Alolayan R.A., Derafa W., Zahou F.M., Bakr R.B. Synthesis of chalcones derivatives and their biological activities: a review. *ACS omega*, 2022, **Vol. 32**, p. 27769-27786. DOI: 10.1021/acsomega.2c01779
33. Shi D., Xu W., Wong M., Popovich D.G. An improved purification method for removing colour interference from 3-(4, 5-dimethylthiazol-2-yl)-2, 5-diphenyl tetrazolium bromide (MTT) antibacterial assays. 2023, *Applied Sciences*, **Vol. 8**, 5067. DOI: 10.3390/app13085067
34. Mahdi Saleh M., Hamid Juma F. Synthesis, Characterization, and Study of Biological, Laser, Nanoscale, Cancer, and Molecular Docking Activity of Tetrazole Compounds Derived from 1, 3, 4-Oxadiazole. In *Macromolecular Symposia,* 2025, **Vol. 414**, 2400219. DOI: 10.1002/masy.202400219